

Article

On the Transferability of Fatigue and Cyclic Deformation Data to 100 μm Thin Structures

Florian Himmelbauer ^{1,*} , Gerhard Winter ¹, Florian Grün ¹  and Constantin Kiesling ²¹ Chair of Mechanical Engineering, Montanuniversität Leoben, Franz Josef-Strasse 18, 8700 Leoben, Austria² LEC GmbH, Inffeldgasse 19, 8010 Graz, Austria

* Correspondence: florian.himmelbauer@unileoben.ac.at; Tel.: +43-3842-402-1411

Abstract: The fatigue properties and cyclic deformation behaviour of materials are usually determined using cylindrical specimens (e.g., $\varnothing 7.5$ mm). Since the transferability to very small dimensions has not been comprehensively considered so far, this study investigates the transferability of specimen data from high-strength steel X5CrNiCuNb16-4 to real structures characterised by a wall thickness of 100 μm . Regarding fatigue, extensive calculations demonstrate that for notched specimens and thin structures, both the material-mechanical support factor concept according to the FKM guideline and the point method of the Theory of Critical Distance (TCD) make correct predictions of the local fatigue strength, with a maximum deviation from experimental values of less than 5%. However, the study points out that the TCD is only conditionally applicable for thin-walled structures, as the material parameter a_0 must be significantly smaller than the wall thickness. Regarding the deformation behaviour, the material reveals special flow characteristics in the first hysteresis. Nevertheless, a combined hardening approach is suitable for modelling. The validation of the model by a plastic deformation of the structure seems plausible, although geometric influences prove to be dominant. In conclusion, even 100 μm thin structures can be evaluated using conventional specimen tests and established assessment or modelling methods.



Citation: Himmelbauer, F.; Winter, G.; Grün, F.; Kiesling, C. On the Transferability of Fatigue and Cyclic Deformation Data to 100 μm Thin Structures. *Metals* **2022**, *12*, 1524. <https://doi.org/10.3390/met12091524>

Academic Editor: Alberto Campagnolo

Received: 1 August 2022

Accepted: 12 September 2022

Published: 15 September 2022

Publisher's Note: MDPI stays neutral with regard to jurisdictional claims in published maps and institutional affiliations.



Copyright: © 2022 by the authors. Licensee MDPI, Basel, Switzerland. This article is an open access article distributed under the terms and conditions of the Creative Commons Attribution (CC BY) license (<https://creativecommons.org/licenses/by/4.0/>).

Keywords: transferability; thin-walled structures; fatigue strength assessment; theory of critical distance; support factor; material modelling; combined hardening model

1. Introduction

The experimental determination of the fatigue strength of real components or parts is a time-consuming and cost-intensive task. Besides the challenging implementation of a suitable testing methodology, the requirements for the experimental determination of the fatigue strength are high, e.g., stable testing conditions, exact experimental and simulation-based definition of the load and stress, sufficient number of tested components, etc.

For this reason, the classical approach is to determine the fatigue strength of a material by tension–compression or rotating bending tests using standardised cylindrical or flat specimens. Influences on the fatigue strength, such as mean stress, notch influence, size influence, temperature, residual stresses, roughness, surface treatment, etc., are investigated using appropriate testing techniques and specimens. Finally, the fatigue strength of the real component is then deduced from the results of the specimen tests, taking into account the relevant approaches [1–6]. Design codes, such as the highly regarded FKM guideline [7], consider these influences.

For the high-strength stainless steel X5CrNiCuNb16-4 used, many properties of the material in different heat treatment conditions, including static and high cycle fatigue (HCF) properties at room and elevated temperatures [8], very high cycle fatigue (VHCF) properties [9–12], fatigue crack growth behaviour [13,14], defect tolerance [15–17], influence of test frequency [10,14,18], size effect [19,20], notch influence [20], influence of corrosive environments [21], influence of the additive manufacturing process on the cyclic deformation and fatigue behaviour [22–24], etc., have been researched by numerous authors.

Notches in real components play a decisive role in the fatigue process. There are numerous approaches to evaluate notched structures, e.g., support factor concepts, respectively, stress gradient-based approaches [7,25], the Theory of Critical Distance (TCD) by Taylor [26], approaches based on the strain energy density [27], energy field intensity approaches [28,29], concepts based on the weakest-link theory [30,31], probabilistic models [32,33], among others. Spaggiari et al. [34] present a comparison between the TCD and the classical stress gradient based approach for the fatigue assessment of notched components and point out the advantages and disadvantages of the approaches. A review of the methods mentioned above is provided by Mei et al. [35]. In numerous studies, notched structures and components are investigated and assessed using stress gradient-based approaches [36,37], or the TCD [38–40]. However, these examined specimens, structures or components have dimensions or wall thicknesses in the range of a few millimetres or even more. There are some studies that use miniaturised specimens and investigate their fatigue behaviour [41–43] and fatigue crack propagation properties [44–46]. However, again, the dimensions considered are in the millimetre range. To the authors' best knowledge, there are no comprehensive investigations that test and assess fatigue properties of very thin structures with wall thicknesses down to the micrometre range.

Especially in the case of notched components with high mean stress conditions, the linear elastic range can be locally exceeded, leading to plastic deformations. For the dimensioning and design of components or structures, knowledge about the constitutive equation of the material is therefore important, as it provides the relationship between the strains and stresses, whether in the elastic or plastic range [47]. A standard model for describing cyclic deformation behaviour is the Chaboche model [48], which combines an isotropic and kinematic hardening approach. A review of various constitutive theories is given in reference [47]. The testing and material modelling are again based on standardised specimens and it is assumed that the occurring stress–strain paths in the real component can be reproduced with sufficient accuracy.

For common technical applications in mechanical engineering, the specimen size is small or similar in size compared to the real component. However, the transferability of the specimen results to real components, as described above, has to be critically questioned, if the dimensions of the real component are significantly smaller or larger than those of the specimen. Hence, the focus of this study is to investigate the transferability of conventional specimen results to real, thin, complex shaped components. In this specific case, very thin-walled (minimum wall thickness 100 μm), notched (radius 0.25 mm) structures are dealt with. The fatigue strength for 10^7 cycles and the cyclic deformation behaviour are examined. The structure of the chapters is also based on these two aspects.

- Transferability of fatigue data to 100 μm thin structures:
The suitability of two fatigue strength assessment approaches is discussed and compared. A local assessment concept according to the FKM guideline [7], which is based on the relative stress gradient and the support effect, and Taylor's TCD [26] are dealt with in detail.
- Transferability of cyclic deformation data to 100 μm thin structures:
The suitability of a standard constitutive model for thin structures is discussed. For this purpose, the structure is specifically plastically deformed and then the calculated and measured displacements are compared.

The current paper provides insights into the applicability of these established fatigue assessment and material modelling methods even for very challenging component geometries. This saves future expensive and time-consuming tests of the real components.

2. Material and Methods

This section describes the simulation and experimental techniques and briefly introduces the fatigue strength assessment approaches as well as the approach for modelling the cyclic deformation behaviour.

2.1. Material

The precipitation hardening steel X5CrNiCuNb16-4, also known as 17-4PH, is used for the investigations. The mechanical properties of this high-strength stainless steel can be widely varied by a heat treatment (solution annealing and precipitation hardening). For example, ASTM A564 [49] specifies minimum yield strengths $R_{p0.2}$ between 520 MPa and 1170 MPa, minimum tensile strengths R_m between 795 MPa and 1310 MPa and elongations A between 10% and 18%. The chemical composition according to DIN EN 10088-3 [50] is shown in Table 1.

Table 1. Chemical composition of the precipitation hardening steel X5CrNiCuNb16-4 in percent by weight (wt%) [50].

	C	Si	Mn	P	S	Cr	Mo	Ni	Cu	Nb
min.	-	-	-	-	-	15.0	-	3.0	3.0	5 × C
max.	0.07	0.7	1.5	0.04	0.03	17.0	0.6	5.0	5.0	0.45

2.2. Fatigue Testing and Assessment

2.2.1. Experimental Procedure

Tension–compression fatigue tests at a stress ratio $R = -1$ were carried out at room temperature (RT) with servo-hydraulic test rigs (Instron Sinus Hydropuls 100/25, ± 100 kN and Instron Structural Testing, ± 50 kN). Conventional HCF tests were performed with unnotched, mildly notched and sharply notched specimens with a test cross-section of $\varnothing 4.0$ mm and $\varnothing 7.5$ mm. For all specimens, the surface in the test area was polished ($R_a = 0.4$ μm). The test frequency was 30 Hz and at 10^7 cycles the specimen was counted as a run-out. Figure 1 shows representative specimen geometries of the $\varnothing 4.0$ mm specimen series and Table 2 summarises the geometric properties of the other specimens. The stress concentration factor K_t and the relative stress gradient χ' were determined with a finite element (FE) simulation, as detailed in Section 2.2.3.

High-frequency VHCF tests (RT, $R = -1$) with mildly notched specimens ($\varnothing 2.5$ mm) and thin-walled structures were conducted on an electrodynamic shaker i210 from IMV Europe Ltd. (München, Germany) using test setups and procedures developed at the Chair of Mechanical Engineering at the Montanuniversität Leoben [10,51,52]. Again, the surface in the test area was polished ($R_a = 0.4$ μm) for all specimens and structures. The test frequency for the specimen tests was in the range of 928 ± 8 Hz and at 10^9 cycles the specimen was counted as a run-out.

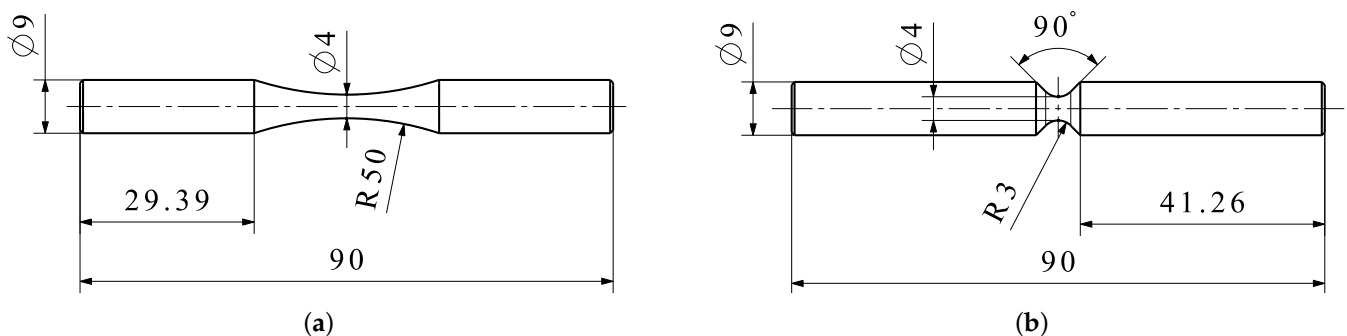


Figure 1. $\varnothing 4.0$ mm specimen geometries for HCF testing: (a) Unnotched specimen. (b) Mildly notched specimen (dimensions in mm).

Table 2. Summary of the geometry characteristics of the specimens and the thin structure, and indication of the number of tested specimens per test series.

Test Series	Notch Radius ρ in mm	Stress Concentration Factor K_t	Rel. Stress Gradient χ' in mm^{-1}	Number of Tested Specimens
Ø4.0, unnotched	50	1.02	0.03	21
Ø4.0, mildly notched	3	1.28	0.56	13
Ø4.0, sharply notched	0.5	2.32	3.88	12
Ø7.5, unnotched	50	1.03	0.03	17
Ø7.5, mildly notched	5.6	1.28	0.31	14
Ø7.5, sharply notched	0.5	3.01	3.97	16
Ø2.5, mildly notched	4.5	1.11	0.37	35
Thin structure	0.25	not definable	26.00	12

A special thin-walled structure, inspired by a practical application, was designed by the authors [51]. The geometric dimensions can be observed in Figure 2a. For the fatigue testing of this structure, it is clamped at the outer edge of the disc. An axially oscillating eigenmode is excited by the shaker, causing the central thickening to be strongly deflected. The cyclic deformation fatigues the inner circumferential notch. The stress distribution in the fatigue critical zone (FCZ) resulting from an upward deflection of the central thickening is also presented in Figure 2b. The test frequency was between 1554 Hz and 1686 Hz, depending on the resonant frequency of the individual structure. Small geometric deviations, such as manufacturing tolerances, have a strong effect on the resonant frequency and notch stress. A resonant frequency drop of 1% was defined as an abort criterion. At 10^9 cycles, the structure was counted as a run-out.

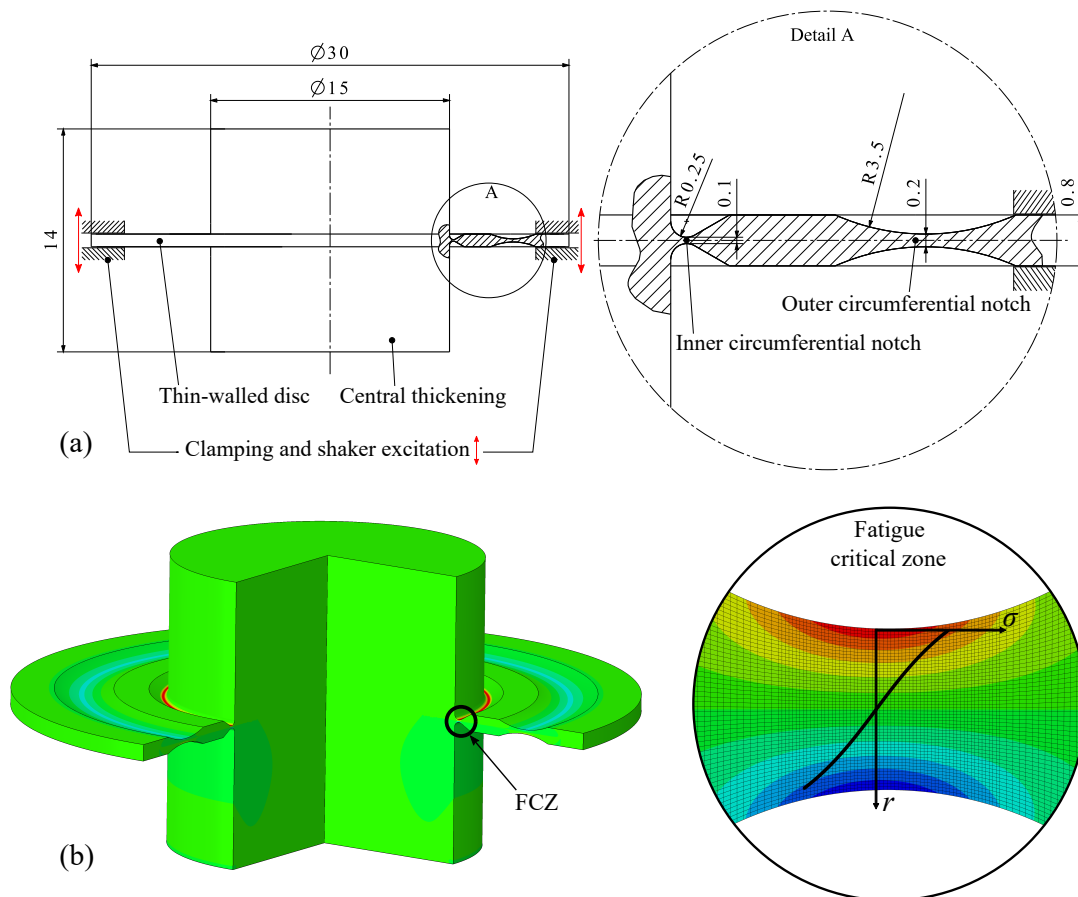


Figure 2. Thin-walled structure for fatigue testing: (a) Geometric dimensions (in mm) and labelling of the main parts. (b) General stress distribution resulting from an upward deflection of the central thickening (sectional view) and detail of the stress distribution in the fatigue critical zone (FCZ).

A total of 93 conventional HCF tests, 35 high-frequency fatigue tests and 12 tests with the structures were carried out, compared in Table 2. Detailed information on the tests with unnotched and notched specimens as well as with thin-walled structures can be found in the study by the authors [20]. Previously published fatigue test results from reference [20] are used in this study for more advanced analysis and interpretation.

2.2.2. Test Evaluation and Processing

The specimens were tested on the basis of nominal stresses in the unnotched or notched test cross-section. The fatigue tests were statistically evaluated using the $\arcsin\sqrt{P}$ transformation [53,54]. All fatigue strength values refer to a survival probability of $P_s = 50\%$. All stress values are presented in normalised form and refer to the measured yield strength $R_{p0.2}$.

For the evaluation of the tests, the local stresses in the notch were used in addition to the nominal stresses. The local stress conditions in the notch were calculated with FE simulations, as detailed in Section 2.2.3. The longitudinal stress (corresponding to the maximum principal stress) was primarily considered.

2.2.3. FE Simulation

FE analyses were carried out using Simulia's Abaqus CAE. Axially symmetrical models of the specimens and the structure were built, and 8-node biquadratic axisymmetric quadrilateral elements (CAX8) were used for meshing. Due to the 2D model, it was possible to mesh very finely, and a special focus was on the notched areas, which were partitioned accordingly. For the notched specimens, a minimum node spacing of 4 μm was used in the notch root. The fatigue critical 100 μm thin zone of the structure was meshed with a node spacing of 1 μm . Nevertheless, due to the axially symmetrical model, the computational effort or computational time was low. Table 3 lists the material parameters of Young's modulus E , Poisson's ratio ν and density ρ . The constitutive model is linear elastic, isotropic and homogeneous.

Table 3. Material parameters used for the linear elastic FE simulations.

E in GPa	ν	ρ in g cm^{-3}
200	0.3	7.8

Static analyses were performed to determine the linear elastic stress distribution in the unnotched and notched specimens. For this purpose, a uniaxial load was applied, causing a nominal stress of 1 MPa in the test cross-section. The calculated stress concentration factor K_f and the relative stress gradient χ' are summarised for each specimen geometry in Table 2.

The small dimensions of the structure make an experimental stress analysis with strain gauges impossible. A simulation approach is therefore essential for determining the stress on the structure due to a given deformation. For each individual structure, static analyses were carried out to determine the stress distribution at a defined deflection of the central thickening. Additionally, modal analyses were conducted using the Lanczos eigensolver. The structures were measured optically (two confocal white light sensors) with a resolution in the micrometre range for an exact representation of the geometry. Due to the small dimensions, it is not possible to validate the calculated stresses or strains with strain gauges, so the FE model of the structure was validated by comparing the experimental and calculated resonant frequencies of each structure. Further information on the simulation techniques and the validation process can be found in reference [20].

2.2.4. Local Fatigue Strength Assessment Concept (FKM Guideline)

According to the FKM guideline [7], the local fatigue strength of a component σ_{LLF} can be determined from the tension–compression fatigue strength of the unnotched specimen

$\sigma_{LLF,0}$ and a design factor K_{WK} . If the roughness of the specimen and the component is comparable and if there is no surface hardening, the design factor is reduced to the support factor n , which takes into account the influence of the stress gradient. The local fatigue strength of the component can therefore be calculated as:

$$\sigma_{LLF} = \sigma_{LLF,0} \cdot n \quad (1)$$

The FKM guideline [7] proposes two support factor concepts for the fatigue strength assessment, that is the older approach of Stielor and the newer material-mechanical support factor. Figure 3 shows a comparison of the two support factor concepts as a function of the relative stress gradient χ' for the investigated high-strength stainless steel. The curves for Stielor's approach refer to the ultimate tensile strength specifications according to ASTM A564 [49]. The material-mechanical support factor is composed of a statistical ("st"), deformation-mechanical ("dm") and fracture-mechanical ("fm") part, see Equation (2). For the current investigations, only the latter two proportions are considered, i.e., $n_{st} = 1$ is assumed, as fatigue results in reference [20] indicate that there is no significant difference between $\varnothing 2.5$ mm, $\varnothing 4.0$ mm and $\varnothing 7.5$ mm specimens. Measured material parameters, such as Young's modulus E , the fatigue strength of the unnotched specimen $\sigma_{LLF,0}$ and the ultimate tensile strength R_m , are used for the calculations. Equations (3) and (4) display the definitions of the deformation-mechanical support factor n_{dm} and fracture-mechanical support factor n_{fm} . The definitions of the endurable alternating plastic strain $\varepsilon_{pl,W}$, the reference tensile strength $R_{m,bm}$ and the exponent n' are given in the FKM guideline [7]

$$n = n_{st} \cdot n_{dm} \cdot n_{fm} \quad (2)$$

$$n_{dm} = \sqrt{1 + \frac{E \cdot \varepsilon_{pl,W}}{\sigma_{LLF,0}} \cdot (n_{st})^{\left(\frac{1}{n'} - 1\right)}} \quad (3)$$

$$n_{fm} = \max \left(\frac{5 + \sqrt{\chi' \cdot \text{mm}}}{5 \cdot n_{dm} \cdot n_{st} + \frac{R_m}{R_{m,bm}} \sqrt{\frac{7.5 + \sqrt{\chi' \cdot \text{mm}}}{1 + 0.2 \cdot \sqrt{\chi' \cdot \text{mm}}}}} ; 1 \right) \quad (4)$$

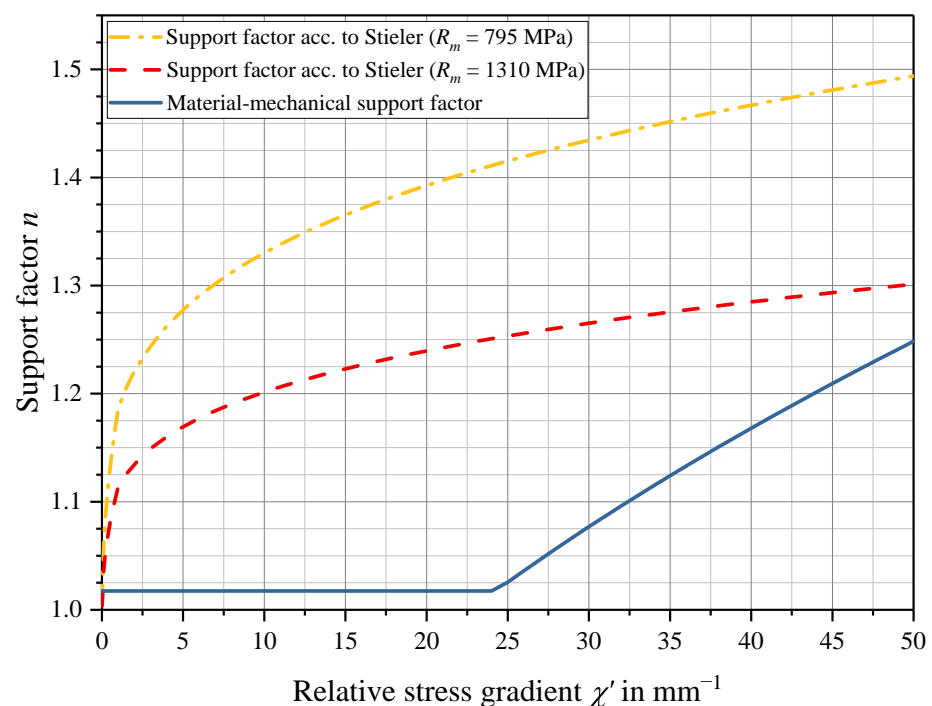


Figure 3. Comparison of the support factor concepts according to the FKM guideline [7] for the high-strength stainless steel X5CrNiCuNb16-4.

For technically relevant values of the relative stress gradient χ' , the support factor according to Stielor is significantly higher than the material-mechanical support factor. Since the material is a high-strength steel, which generally have only a low support effect, the material-mechanical support factor concept is considered to have more practical relevance. The increase in the material-mechanical support factor at very high relative stress gradients, that is $\chi' > 24 \text{ mm}^{-1}$, is due to the increasing influence of the fracture-mechanical part.

2.2.5. Theory of Critical Distance

To describe the fatigue strength behaviour of cracks and notches, a unified approach, called the Theory of Critical Distance, was proposed by Taylor [26]. The basic idea is that the stress or stress distribution at a certain distance from the notch root or the crack tip is decisive for the fatigue strength assessment. In applying this theory, Taylor distinguishes between the so-called point, line and area method of the TCD. There are also volume-based approaches of the TCD [55]. The point and line method are considered in the course of this work. The point method states that when $\Delta K = \Delta K_{th}$, that is the stress intensity factor range equals the threshold value, the elastic stress σ_{eff} at a distance $r = a_0/2$ from the notch root or from the crack tip is equal to the fatigue strength of the unnotched specimen $\sigma_{LLF,0}$, see Equation (5).

$$\sigma_{eff} = \sigma(r = a_0/2, \theta = 0) = \sigma_{LLF,0} \quad (5)$$

Instead, the line method determines an average stress σ_{av} by integrating along a line from the notch root/crack tip $r = 0$ to $r = 2a_0$, and then sets this average stress equal to the fatigue strength of the unnotched specimen $\sigma_{LLF,0}$, see Equation (6).

$$\sigma_{av} = \frac{1}{2a_0} \int_{r=0}^{2a_0} \sigma(r, \theta = 0) dr = \sigma_{LLF,0} \quad (6)$$

Both definitions refer to the notch root or crack plane, i.e., $\theta = 0$. Therefore, it is not the maximum notch stress or stress at the crack tip, but the stress σ_{eff} at the distance $r = a_0/2$ or the average stress σ_{av} along a line from $r = 0$ to $r = 2a_0$ that is relevant for the fatigue assessment.

The material parameter a_0 was proposed by El Haddad et al. [56] and is calculated according to Equation (7). The threshold stress intensity factor range ΔK_{th} was not determined experimentally in the current investigations, instead, the value given by Schönbauer et al. [21] for 17-4PH (condition H1150), $\Delta K_{th} = 6.7 \text{ MPa}\sqrt{\text{m}}$ for $R = -1$, is used.

$$a_0 = \frac{1}{\pi} \left(\frac{\Delta K_{th}}{\Delta \sigma_{LLF,0}} \right)^2 \quad (7)$$

The calculated material parameter a_0 has a value of only a few micrometres for the investigated high-strength steel. For a meaningful and reliable assessment, the fatigue critical zone must therefore be extremely finely meshed in the FE analysis in order to be able to calculate the stress distribution in the notch root with sufficient accuracy. As already stated in Section 2.2.3, a node spacing of $1 \mu\text{m}$ is chosen for the simulations of the structures. Figure 2b illustrates the meshing and the stress distribution in the FCZ. The nominal wall thickness in the FCZ is $100 \mu\text{m}$.

2.3. Testing and Modelling of the Cyclic Deformation Behaviour

2.3.1. Experimental Procedure: Specimens

Strain-controlled low cycle fatigue (LCF) tests were performed at RT on a servo-hydraulic test rig (Instron Sinus Hydropuls 100/25, $\pm 100 \text{ kN}$), the strain was measured using an Instron extensometer type 2620-601 (reference length $l_0 = 12.5 \pm 5 \text{ mm}$). Unnotched specimens with a test section of $\text{Ø}7 \text{ mm} \times 20 \text{ mm}$ were tested, see Figure 4. The tests were carried out with a strain rate of $1\%/s$ and the strain ratio was $R_\epsilon = -1$. Total

specimen fracture was chosen as the failure criterion. In addition to the standard LCF tests, some supplementary strain-controlled tests with a defined strain path were carried out to improve the knowledge of the material's deformation behaviour. A total of 19 LCF tests were conducted.

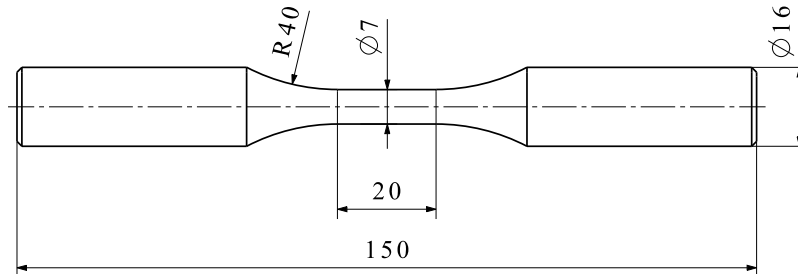


Figure 4. Specimen geometry for strain-controlled LCF tests (dimensions in mm).

2.3.2. Modelling of the Cyclic Deformation Behaviour

For a numerical simulation of the cyclic deformation behaviour, a mathematical model is necessary. In this study, the elasto-plastic material behaviour of the high-strength steel X5CrNiCuNb16-4 is described with a Chaboche model [48]. This is a combined hardening approach and includes an isotropic and a kinematic part. The yield function f of this model is shown in Equation (8). The term $J(\sigma - X)$ denotes the von Mises criterion, which is specified in Equation (9). Here, σ is the stress tensor and X is the kinematic stress tensor, σ' and X' are the respective deviatoric components. The initial size of the yield surface is represented by the variable k and R is the parameter for the isotropic hardening model. For $f < 0$, the material behaviour is linear elastic, while $f = 0$ implies plastic flow [48].

$$f = J(\sigma - X) - R - k \quad (8)$$

$$J(\sigma - X) = \left[\frac{3}{2} (\sigma' - X') : (\sigma' - X') \right]^{1/2} \quad (9)$$

Isotropic hardening describes the change of the yield surface with respect to its size, but not with respect to its position in the stress space. The increase or decrease in the yield surface is modelled with the parameter R . Equation (10) shows the underlying differential equation for isotropic hardening, with the constants Q and b . By integrating Equation (10), an explicit formula is obtained for the change in the size R of the yield surface as a function of the accumulated plastic strain p , see Equation (11) [48].

$$dR = b(Q - R) dp \quad (10)$$

$$R = Q(1 - e^{-bp}) \quad (11)$$

Kinematic hardening describes the translation of the yield surface in the stress space, the size of the yield surface remains constant. This is expressed by the kinematic stress tensor X . A non-linear approach as described by Chaboche [48] is used. Equation (12) gives the governing differential equation with constants C_i and γ_i of the non-linear kinematic model. By superimposing m identical approaches X_i , the accuracy of the model is improved, see Equation (13). Exclusively in Equation (12), $d\varepsilon_p$ represents the plastic strain rate and dp is calculated as $dp = (\frac{2}{3} d\varepsilon_p : d\varepsilon_p)^{1/2}$ [48].

$$dX_i = \frac{2}{3} C_i d\varepsilon_p - \gamma_i X_i dp \quad (12)$$

$$X = \sum_{i=1}^m X_i \quad (13)$$

For uniaxial loading, the integration of Equation (12) with the initial values ε_{p0} and $X_{0,i}$ gives Equation (14). The variable $\nu = \pm 1$ indicates the direction of the flow [48,57].

$$X_i = \nu \frac{C_i}{\gamma_i} + \left(X_{0,i} - \nu \frac{C_i}{\gamma_i} \right) e^{-\nu \gamma_i (\varepsilon_p - \varepsilon_{p0})} \quad (14)$$

A newly developed optimisation routine, which was set up with the software MATLAB from MathWorks, automatically determines the material model parameters from the hystereses of LCF tests. These parameters can be used in conventional FE solvers. The methodology for the derivation of the Young's modulus E , the initial yield strength k , the isotropic parameters Q and b and the kinematic parameters C_i and γ_i from experimental data was developed at the Chair of Mechanical Engineering at the Montanuniversität Leoben and was first published by Seisenbacher et al. [58]. An LCF test with high total strain amplitude was used to determine the isotropic and the kinematic parameters. For the isotropic parameters, the cyclic yield strength $R_{p0.005}$ of every cycle is plotted against the accumulated plastic strain and then the isotropic model, Equation (11), is fitted accordingly. For the kinematic approach, the second hysteresis was chosen to derive the parameters, as it is representative for all further hystereses (no further softening). The ascending branch of the stress–plastic strain hysteresis serves as input data for the fit of the kinematic hardening model. A kinematic approach with two back stresses is used, which means $m = 2$ in Equation (13). After the first rough parameter determination, the parameters were optimised with the aim to optimally reproduce the stress–strain behaviour of the first cycle at any total strain amplitude.

Once the parameters had been determined, basic simulations of the cyclic deformation behaviour were carried out using Simulia's Abaqus CAE. A unit cell with element type C3D20R (a 20-node quadratic brick with reduced integration) was modelled for the calculations.

2.3.3. Experimental Procedure: Structures

In order to check the validity of the cyclic deformation model also for 100 μm thin structures, the structure was specifically plastically deformed. For this purpose, the structure was firmly clamped at the outer edge in the same test apparatus [51] used for the fatigue tests. Instead of being connected to the electrodynamic shaker, the test apparatus was placed in the materials' testing machine ZwickRoell Z2.5/TS1S. A single deflection of the structure was investigated, resulting in plastic deformations in the inner and outer circumferential notch. The force was introduced into the central thickening via a punch. The test was performed in a force-controlled manner. The testing machine recorded the force and the displacement of the punch. At the beginning, a calibration measurement was carried out to obtain the stiffness of the load frame of the testing machine. This deformation of the testing machine was compensated in the subsequent analyses.

Figure 5 presents the experimental setup for the plastic deformation of the structure. A more detailed insight into the setup is provided by the simulation model in Figure 6. However, the simulation model only consists of the essential parts.

2.3.4. FE Simulation of the Thin Structure

The basic axially symmetrical simulation model of the structure, see Section 2.2.3, was extended. In addition to the structure, the essential parts of the test setup (base plate, intermediate disc and punch) were also modelled and provided with appropriate contact conditions (penalty formulation with friction coefficient = 0.15). Again, CAX8 elements were used for meshing. The structure was assigned the determined combined hardening material model (compare Section 2.3.2), while the other components were given the material parameters from Table 3.

Besides the material non-linearity, geometrically non-linear behaviour has to be assumed for the simulation of the investigated thin-walled structure. The expected deformations in relation to the undeformed structure make the assumption of a linear strain–displacement relation inadmissible, moreover, the equilibrium equations may no longer

be set up on the undeformed structure [59]. Furthermore, thin plates or structures that are clamped at the outer edge and loaded vertically experience a stress-stiffening effect [60]. Tensile stresses lead to a change in the transverse stiffness of the component, which results in a smaller vertical deflection in a non-linear analysis compared to a linear analysis. For other sources of geometric non-linearity, please refer to the relevant literature. In Abaqus CAE, the option *nlgeom* was therefore activated.

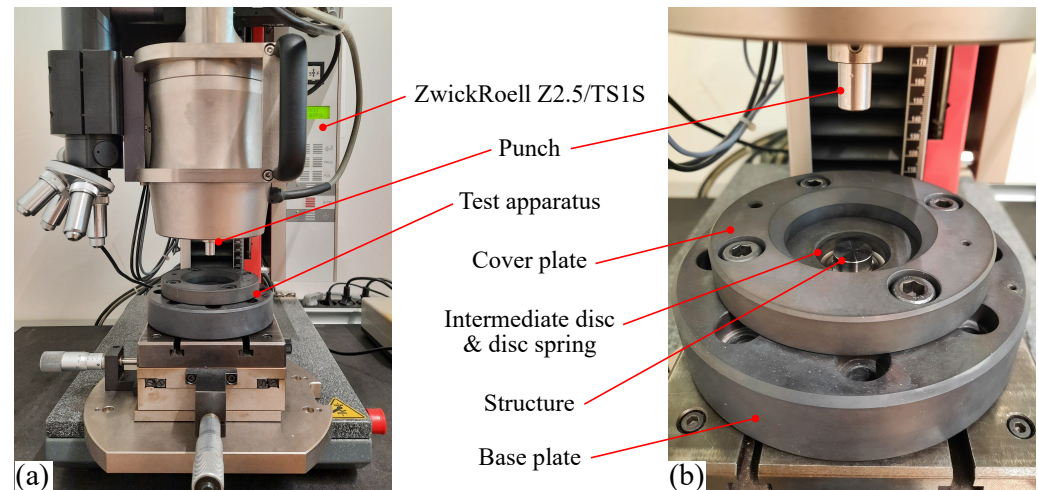


Figure 5. Experimental setup for the plastic deformation of the thin-walled structure: (a) Overview. (b) Detail of the test apparatus with firmly clamped structure.

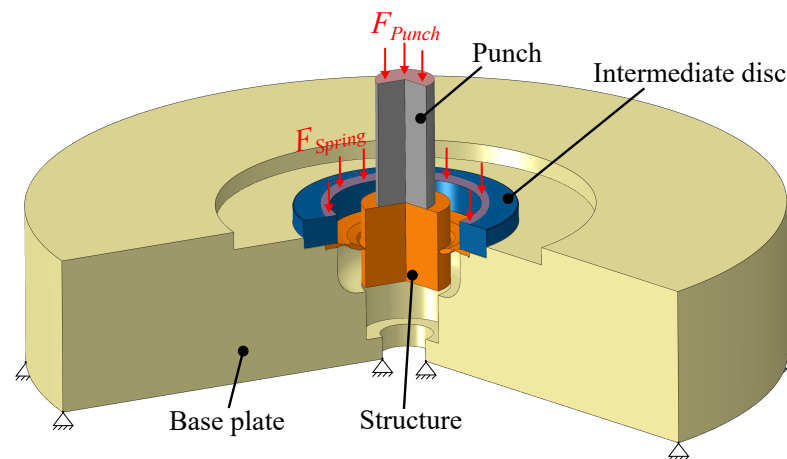


Figure 6. Simulation model for the plastic deformation of the thin-walled structure. The deflection of the structure is exaggerated.

The analysis consists of three steps. Firstly, the preload force F_{Spring} of the disc spring is applied via the intermediate disc, which presses down the outer edge of the structure with approximately 4.4 kN. Then, the force $F_{Punch} = 725$ N is applied via the punch, which moves the central thickening of the structure downwards. In the third step, the force F_{Punch} is reduced to 0 N. Figure 6 illustrates a sectional view of the simulation model during the deformation of the structure, where the deflection of the structure is exaggerated. For the evaluation, the vertical displacement of the punch top and the applied force were used.

3. Results

In this section, firstly, the statistically evaluated fatigue strength values of the un-notched and notched test series are presented and compared with each other. Then, the transferability of the specimen results to thin structures is demonstrated with the help of the support factor concept and the Theory of Critical Distance. Subsequently, the tested and

modelled cyclic deformation behaviour is compared on a specimen basis and, again, the transferability of these deformation data from specimens to much more complex geometries is demonstrated.

3.1. Fatigue Strength: Specimen Results

The statistically evaluated fatigue strength values for 10^7 cycles are considered in the following. In Figure 7, the results of all specimen test series are plotted. The fatigue strength values related to nominal stresses $\sigma_{LLF,nom,norm}$ are displayed in a normalised form as a function of the stress concentration factor K_t . In addition, the dashed line shows the hypothetical fatigue strength of specimens with $K_t > 1$ as a function of K_t starting from the value of the unnotched specimen $\sigma_{LLF,0}$. Since the dashed line and the test results correspond very well, it can be stated that the fatigue notch factor K_f , i.e., the ratio of the fatigue strength of the unnotched to the notched specimen, related to nominal stresses, is equal to the stress concentration factor K_t . Thus, no support effect is observed and the material is classified as fully notch-sensitive.

The application of the nominal stress concept is limited to components and structures, for which a nominal cross-section can be defined. For the thin-walled notched structure, it is therefore not possible to specify a nominal stress. In the case of real components with complex geometry, assessment concepts based on local stresses are more suitable. The stress concentration factor K_t refers to the maximum stress in the notch root in relation to the nominal stress. The maximum stress in the notch root is the longitudinal stress, which is also the maximum principal stress (as there are no shear stresses in the notch root surface). K_t therefore refers to the maximum principal stress. Figure 8 shows a comparable representation to Figure 7, except that the local notch stress in the notch root is now considered. The determined normalised local fatigue strength values $\sigma_{LLF,norm}$ based on the maximum principal stress as a function of the relative stress gradient χ' are displayed. In addition to the specimen series, the local fatigue strength of the thin-walled structure is also plotted.

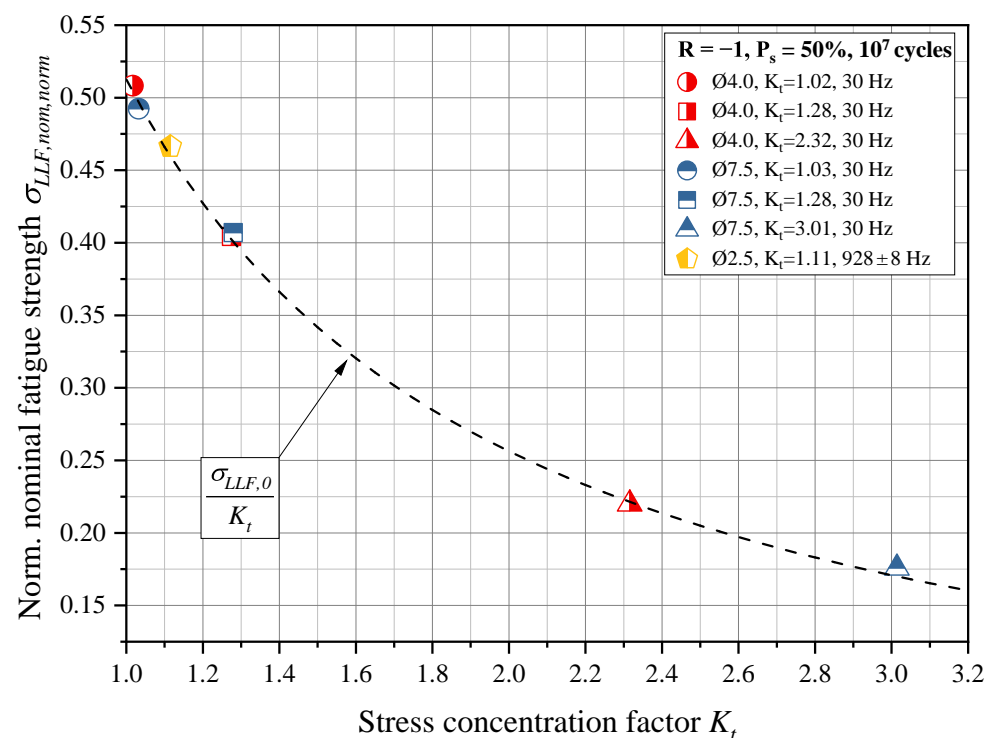


Figure 7. Experimentally determined normalised nominal fatigue strength $\sigma_{LLF,nom,norm}$ against the stress concentration factor K_t .

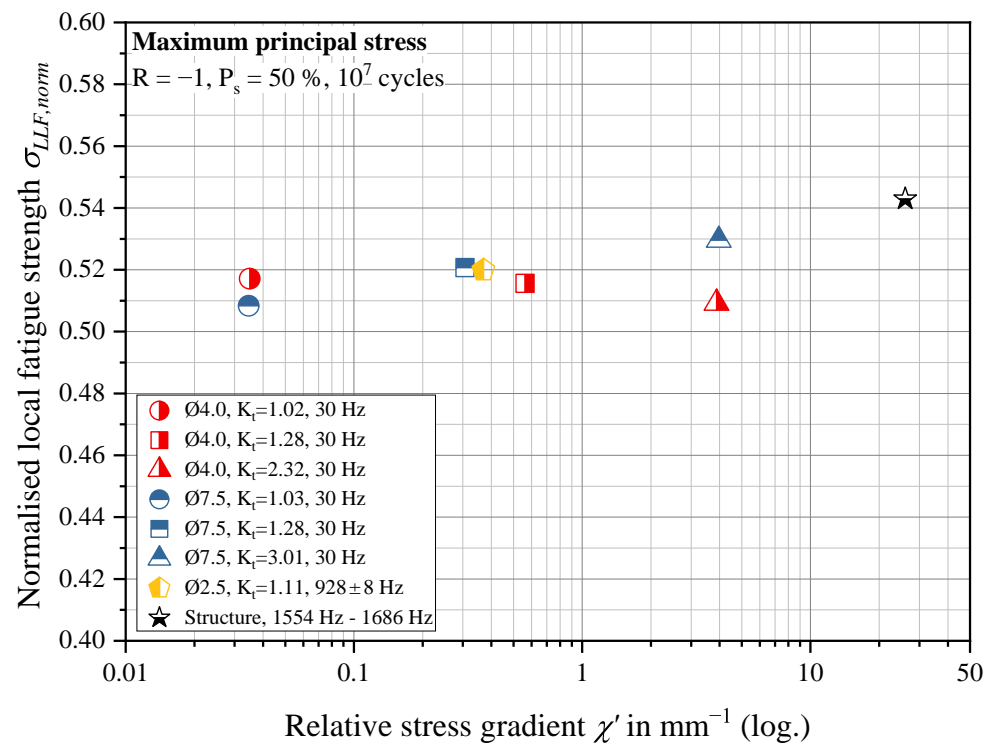


Figure 8. Experimentally determined normalised local fatigue strength $\sigma_{LLF, norm}$ against the relative stress gradient χ' .

Figure 8 clearly shows that regardless of the notch sharpness or the relative stress gradient, the local fatigue strength (maximum principal stress) of the specimens is always very similar $\sigma_{LLF, norm} \approx 0.52$ and there is no pronounced support effect on a specimen basis. The evaluation proves that for the material X5CrNiCuNb16-4, the maximum principal stress governs the fatigue behaviour. A similar statement is made by Schönbauer et al. [61], who tested the torsional fatigue limit of the same material and concluded that the biaxial stress state at the surface is neglectable and only the maximum principal stress determines the fatigue behaviour under torsional loading. Figure 8 also highlights the fact that the thin-walled structure has a slightly higher local fatigue strength than the specimens. This behaviour is studied below using two different approaches.

3.2. Fatigue Strength: Transferability to Structures

In a further step, calculations are made for the fatigue strength assessment of notched specimens and thin-walled structures starting from the fatigue strength of the unnotched specimen. Specifically, the methods from Sections 2.2.4 and 2.2.5 are applied. Three different test cross-sections (Ø2.5 mm, Ø4.0 mm and Ø7.5 mm), two different notch shapes (mildly notched and sharply notched) and the 100 μm thin structure are examined. Figure 9 summarises the entire calculations. The tested or calculated local fatigue strength σ_{LLF} for each individual test series is shown in relation to the fatigue strength of the unnotched specimen $\sigma_{LLF,0}$. In each case, the maximum stress in the notch root is considered.

As already demonstrated in Figure 8, the tests with mildly notched specimens demonstrate almost the same fatigue strength, independent of specimen size or testing technique. The difference in fatigue strength is moderately greater for the sharply notched specimens. Possible causes have already been pointed out by Himmelbauer et al. [20], e.g., manufacturing tolerances, location of the tested stress levels and a statistical influence. On average, the fatigue strength of the sharply notched specimens is again comparable to that of the mildly notched specimens. The local fatigue strength of the thin-walled structures, on the other hand, is significantly higher, specifically by about 6.8% compared to the unnotched specimen series.

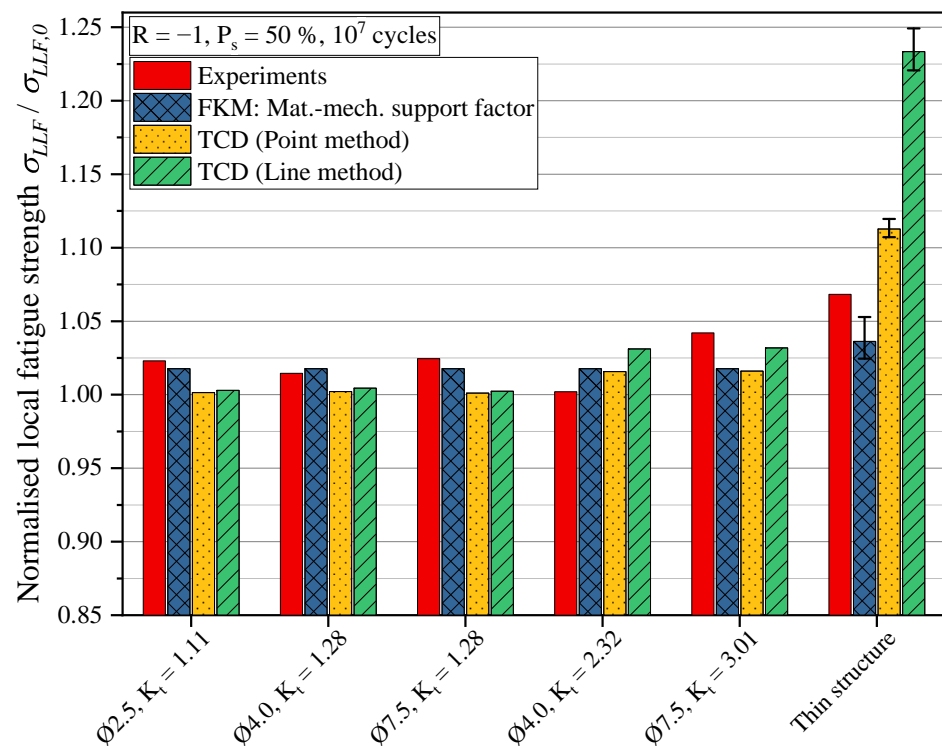


Figure 9. Comparison between the results obtained with different approaches (support factor concept according to the FKM guideline [7] and Theory of Critical Distance (TCD) according to Taylor [26]), for the fatigue strength assessment of notched specimens and thin-walled notched structures. The black bars on the graphs of the structure represent the influence of small geometric deviations, e.g., manufacturing tolerances.

The material-mechanical support factor models this behaviour correctly. As a matter of fact, there is a very low support effect (1.8%) for relative stress gradients $\chi' < 24 \text{ mm}^{-1}$, which applies to the mildly and sharply notched specimens, and at higher relative stress gradients there is a moderate increase in the support effect. A representative value of $n = 1.036$ is calculated for the structure. As shown by Himmelbauer et al. [20,51], small geometric deviations, e.g., due to manufacturing tolerances, have a pronounced effect on the natural frequency and the stress distribution in the fatigue critical zone of the thin-walled structures. The black bars on the graphs of the structure represent this influence of the geometry on the calculated local fatigue strength. Nevertheless, the FKM approach underestimates the fatigue strength of the thin-walled structure by about -3.0% (maximum deviation -4.1% , minimum deviation -1.4%). However, this is a conservative design.

The point method of the TCD gives plausible and conservative values for the mildly and sharply notched specimens. It is interesting to note that both the material-mechanical support factor and the point method of the TCD do not indicate a significant local strength increase for the notched specimens. In contrast, a local fatigue strength in the notch of 1.11 is calculated for the structure compared to the unnotched specimen. The influence of the geometry on the calculated fatigue strength is small. The fatigue strength determined with the point method is $+4.2\%$ (maximum deviation $+4.8\%$, minimum deviation $+3.6\%$) above the experimentally determined fatigue strength of the structure.

The line method of the TCD gives similar results to the point method for the mildly notched specimens, but the difference becomes greater for the sharply notched specimens. The results are still practical. However, when assessing the structure, the line method clearly overestimates the local fatigue strength. The deviation is about $+15.4\%$ (maximum deviation $+16.9\%$, minimum deviation $+14.3\%$).

The calculations confirm that for the fatigue strength assessment of thin-walled structures with a minimum wall thickness of $100 \mu\text{m}$ made of high-strength steel X5CrNiCuNb16-

4, both the local assessment concept according to the FKM guideline and the point method of the TCD are suitable. While the first approach slightly underestimates the local fatigue strength, the second approach overestimates it. Nevertheless, it is important to note that the deviations from the experimentally determined value are less than 5%. This is a very satisfactory result. The line method of the TCD is not recommended for very thin structures, because compared to the other approaches the deviation is noticeably larger.

3.3. Deformation Behaviour: Specimen Results

A comparison between an LCF test with high total strain amplitude A and its corresponding simulation is shown in Figure 10. The normalised stress σ -strain ε hystereses for cycle 1 and cycle $N_f/2$ (half of the number of cycles to failure) are presented. The material shows a special deformation behaviour during initial loading. After a pronounced linear elastic range and a very high initial yield strength, the material exhibits an almost ideal plastic yielding in the first load cycle. However, the deformation characteristics change fundamentally during reverse loading. The cyclic yield strength drops sharply and additionally, there is no longer an ideal plastic behaviour. The cyclic yield strength is practically constant from the second cycle onwards and the maximum stress remains at the initial level. Thus, this precipitation hardening steel does not show cyclic softening after the first cycle. A comparison of the experiments and the simulations confirms that the determined simulation model reproduces the described complex deformation behaviour excellently for each individual cycle.

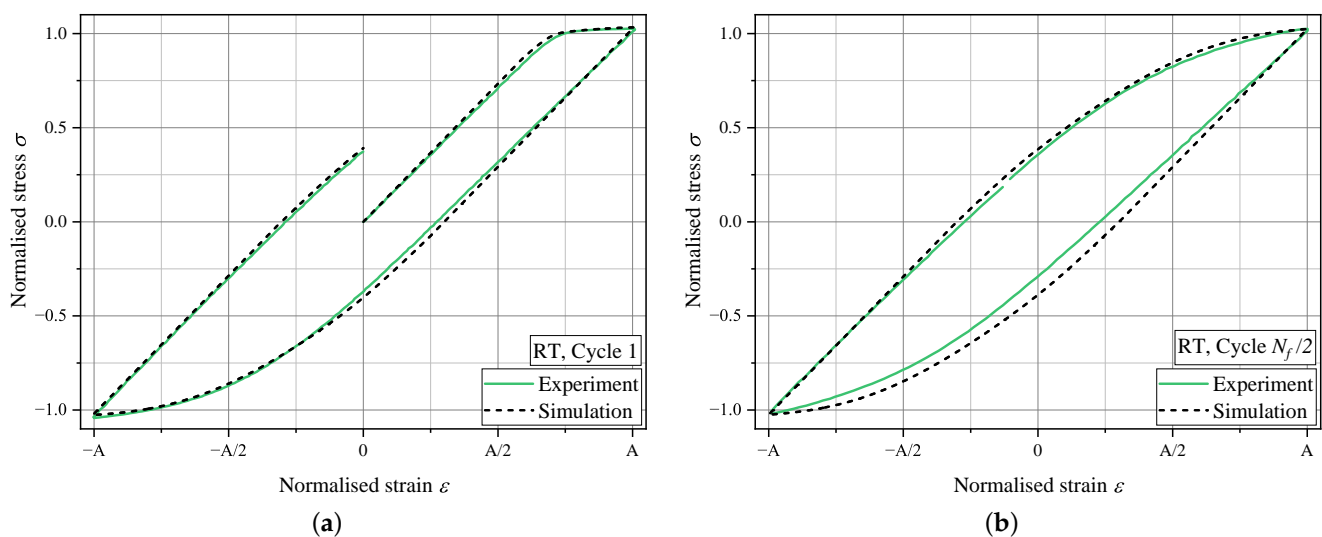


Figure 10. Comparison of the tested and calculated cyclic deformation behaviour at RT for (a) cycle 1 and (b) cycle $N_f/2$ with high total strain amplitude A .

As Figure 11a displays, the previously described elastic-ideal plastic deformation behaviour during initial loading and the changed characteristics during reverse loading also occur with a starting direction in compression. This special yielding property is therefore independent of the loading direction and only appears in the first load cycle. Moreover, it is of practical interest to know how the material responds to very high plastic strains. Figure 11b shows a test with an irregular load history, in which a conventional LCF cycle is followed by a large tensile load. The ideal plastic behaviour reappears at the point of the first load reversal. Again, the derived simulation model superbly reproduces all the mentioned deformation properties of the material.

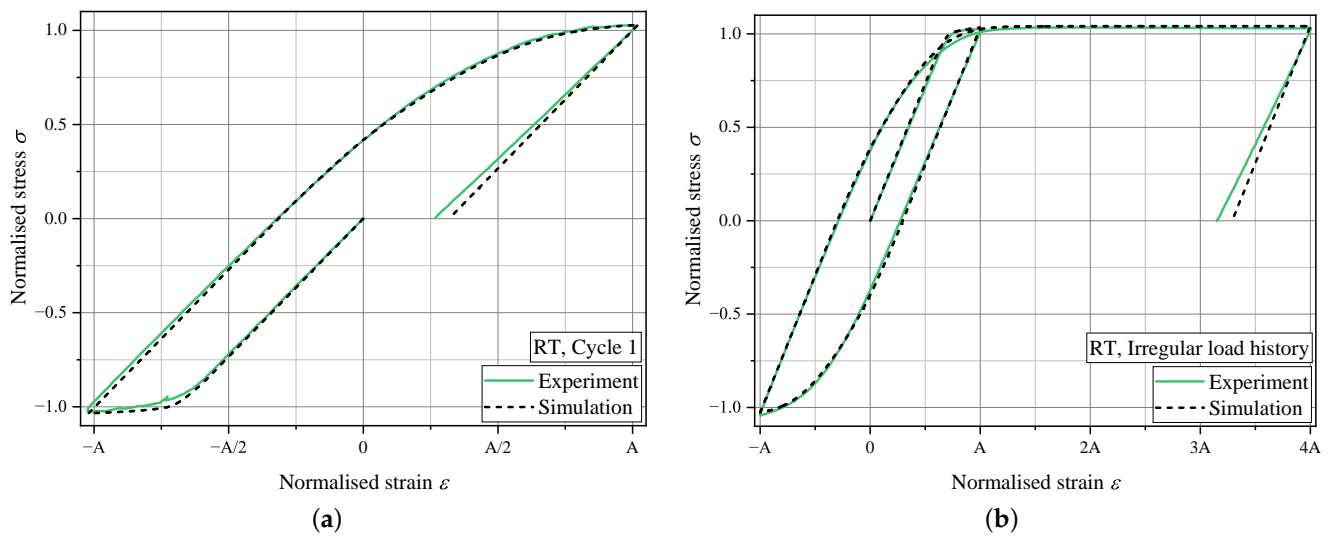


Figure 11. Comparison of the tested and calculated cyclic deformation behaviour at RT: (a) Influence of the starting direction. (b) Irregular load history.

A comparison between an LCF test with low total strain amplitude B and its corresponding simulation is finally presented in Figure 12. The first load cycle with the very high initial yield strength and the moderate plastification during reverse loading are again well modelled. As long as the initial yield strength is not exceeded once, there is no reduction in the cyclic yield strength with accumulated plastic strains. Thus, purely elastic behaviour is correctly reproduced by the model for each cycle.

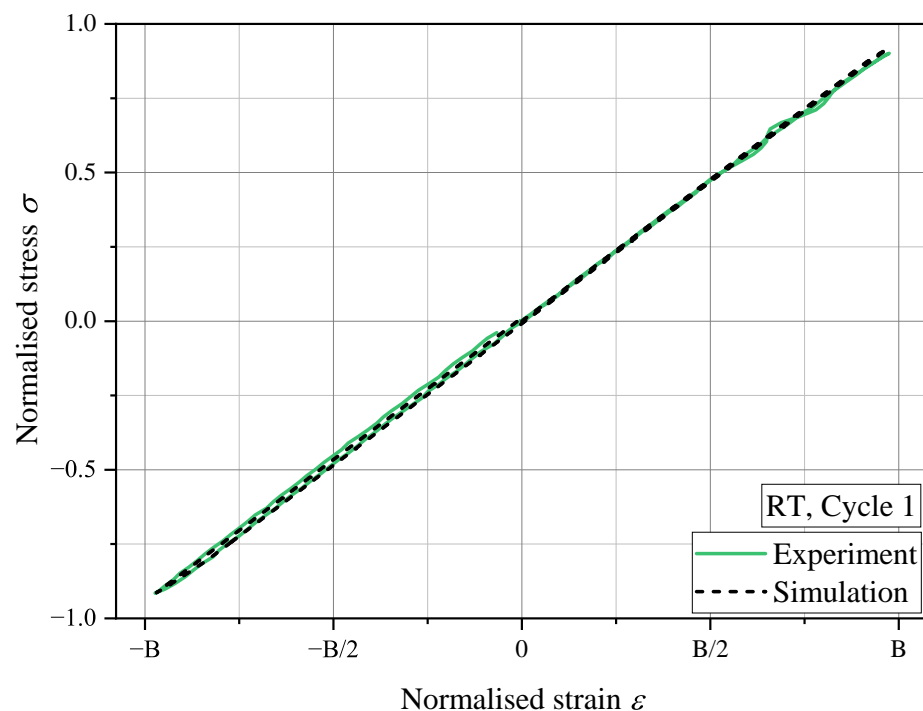


Figure 12. Comparison of the tested and calculated cyclic deformation behaviour at RT for cycle 1 with low total strain amplitude B .

3.4. Deformation Behaviour: Transferability to Structures

The fundamental question in this section is whether the cyclic deformation behaviour obtained on conventional specimens can be applied to $100\ \mu\text{m}$ thin structures. Figure 13 shows an important first finding from a simulation study. Apparently, besides the non-linear material behaviour, the non-linear geometric behaviour also plays a significant role

for these thin-walled structures. A calculation with only the non-linear material model leads to a degressive force-displacement curve (red dotted curve), as this would be expected from the specimen tests. In contrast, a calculation with a linear elastic material model and taking geometric non-linearity into account yields a progressive curve (blue solid curve). The stress-stiffening effect also causes significantly smaller deflections. Additionally, the friction conditions have a noticeable effect, as a hysteresis occurs even with a linear elastic material model. A final calculation with consideration of all sources of non-linearity provides the black dashed hysteresis, which is again markedly different from the other curves. Here, both a progressive force-displacement relation and a permanent plastic deformation occur. A direct validation of the cyclic deformation model is therefore challenging, because the various non-linear influences are difficult to separate.

It is assumed that for the correct representation of the experimental results, the consideration of the material non-linearity, the geometric non-linearity and the friction condition is necessary. Furthermore, the realistic modelling of the geometric dimensions of the structure is very important. As demonstrated in previous studies [20,51], manufacturing tolerances have a large influence on the stress distribution and the natural frequencies. However, even when looking at a single structure, variations in thickness are measured in the circumferential direction. Results of the axially symmetrical simulations with the maximum and minimum measured dimensions are shown in Figure 14. For the analysed structure, there is a measured difference of 8 μm in the wall thickness of the inner circumferential notch (nominal thickness 100 μm), and the difference in the general wall thickness (nominal thickness 0.8 mm) is a maximum of 15 μm . These variations in wall thickness do have a noticeable effect on the force-displacement diagram. The maximum deflection differs by 20 μm . The choice of averaged dimensions seems to be a necessary compromise.

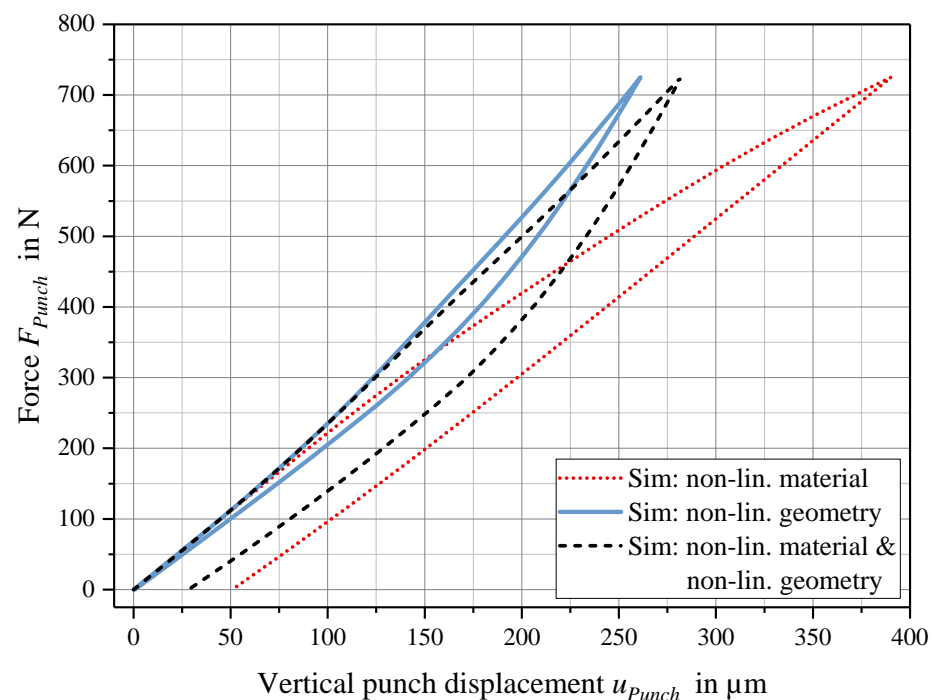


Figure 13. Simulation study on the effects of the non-linear material model and the geometric non-linearity on the resulting force-displacement curve of the punch during a deflection of the thin-walled structure.

The following simulation uses the averaged dimensions as well as the non-linear material behaviour and the geometric non-linearity. A comparison of the experimental and calculated force-displacement curve of the punch is given in Figure 15. The experiment reveals a pronounced progressive behaviour, as predicted by the simulation study. The corresponding simulation maps the force-displacement curve well. In particular, the

maximum displacement is computed precisely, and the difference between experiment and simulation is $4\ \mu\text{m}$. There are minor differences in the permanent plastic deformation between the experiment and simulation ($\Delta 13\ \mu\text{m}$). The application of the cyclic deformation model therefore leads to significant improvements in the simulation of the thin structure.

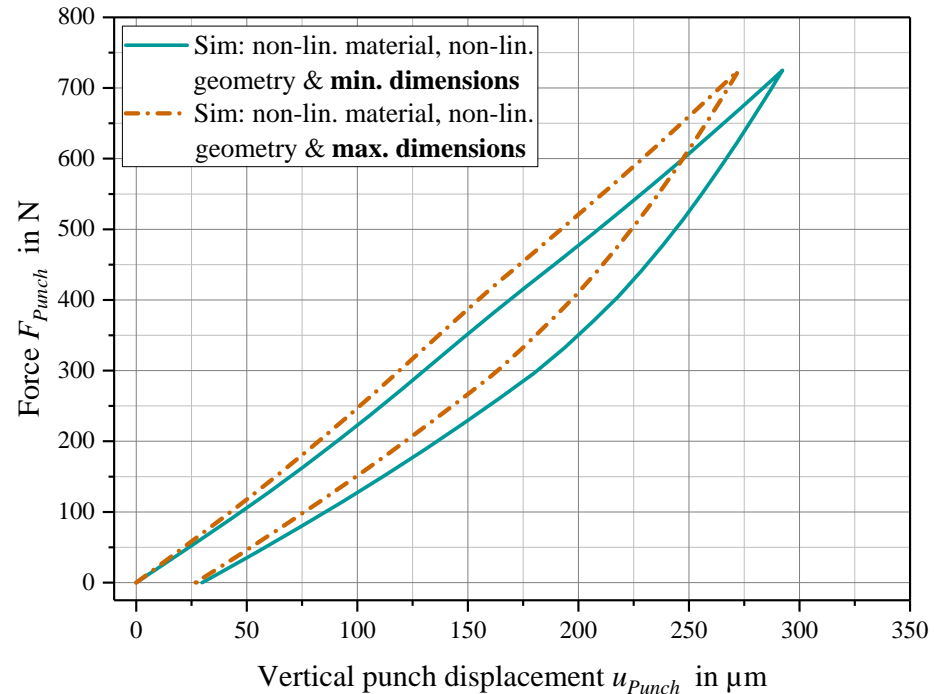


Figure 14. Simulation study on the influence of wall thickness variations, based on measured minimum (min.) and maximum (max.) dimensions for a single structure, on the resulting force-displacement curve of the punch during a deflection of the thin-walled structure. The simulations consider non-linear material behaviour and geometric non-linearity.

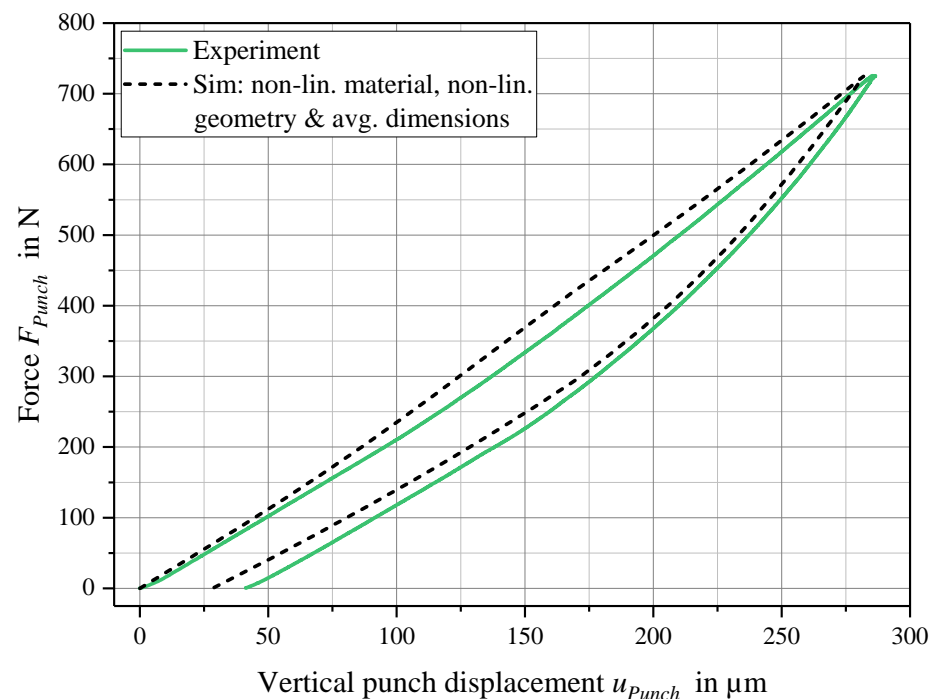


Figure 15. Comparison of the tested and calculated force-displacement curve of the punch during a deflection of the thin-walled structure. The simulation considers non-linear material behaviour, geometric non-linearity and the averaged (avg.) measured dimensions of the structure.

4. Discussion

4.1. Applicability of the TCD for Thin-Walled Structures

The applicability of the TCD for very thin-walled structures must be critically questioned in general. In the current investigation, a structure with a minimum wall thickness of 100 μm made of a high-strength steel is examined. For this material, the parameter a_0 is only a few micrometres, resulting from a comparatively low threshold stress intensity factor range ΔK_{th} and high fatigue strength $\sigma_{LLF,0}$. In the present case, the method is applicable and provides plausible results.

However, if the same structure is made from a different material, resulting in a significantly larger value for a_0 , the TCD would no longer be applicable for the thin-walled structure. Characteristic values for a_0 are given in references [62–65], among others, and range from 5 μm for high-strength steels, 0.3 mm for mild steels to 3 mm for grey cast iron. Either the calculation is not possible because a_0 is greater than the wall thickness or, if a_0 is smaller than the wall thickness, the stress at the considered location ($r = a_0/2$) has no physical meaning for the fatigue strength assessment (think of a thin bending beam, where for the assessment of the tensile side the effective stress $\sigma_{eff} = \sigma(r = a_0/2)$ is already a compressive stress).

It has to be noted that the TCD calculations for the thin-walled structure are only valid and plausible because the parameter a_0 is correspondingly small. The larger deviations with the line method already indicate that the range $r = 0$ to $r = 2a_0$ over which the stress is averaged is too large compared to the wall thickness of the structure. Since the TCD seems to provide practical results for 100 μm thin structures only for high-strength materials, a support factor concept based on the relative stress gradient is more preferable for these types of thin-walled structures.

In principle, thin structures show comparable fatigue properties to conventional specimens. The slightly increased local strength can be explained with known concepts, e.g., support effect approaches. The transferability of specimen fatigue data to thin-walled structures characterised by a wall thickness of 100 μm and made of X5CrNiCuNb16-4 can therefore be confirmed. An ongoing study by the authors also confirms the transferability in the VHCF regime and at elevated temperatures.

4.2. Transferability of the Deformation Behaviour

The transferability of conventional specimen deformation data to thin-walled structures seems to be given in principle, but the comparatively high forces and displacements lead to a number of additional effects. The consideration of geometric non-linearity in the simulation, the realistic representation of the geometrical dimensions of the structure and the modelling of the friction conditions require more detailed FE analyses. The influences mentioned make it difficult to validate the cyclic deformation model on its own.

In addition to the challenges in the simulation, there are also challenges in the experimental setup. The clamping of the structure in the test apparatus and the measurement of the very small displacements in the micrometre range are worth mentioning here. Under all these aspects, one can speak of a satisfactory agreement between the experiment and simulation, as compared in Figure 15. A detailed measurement of the structure before and after the plastic deformation and a comparison of the contour with the simulation could eliminate uncertainties in the measurements of the testing machine and provide further clarity.

The cyclic deformation model contributes to a significant improvement and the occurring stress–strain paths can certainly be mapped more realistically. Nevertheless, the exact representation of the geometric dimensions and the treatment of the geometric non-linearity have a major impact on these thin structures characterised by a wall thickness of 100 μm . However, the transferability of the cyclic deformation behaviour from conventional specimens to thin-walled structures seems to be given.

5. Conclusions

This study deals with the transferability of conventional specimen data ($\varnothing 2.5$ mm, $\varnothing 4.0$ mm, $\varnothing 7.0$ mm and $\varnothing 7.5$ mm) to very thin structures characterised by a minimum wall thickness of 100 μm and made of high-strength stainless steel X5CrNiCuNb16-4. Specifically, the fatigue strength for 10^7 cycles and the cyclic deformation behaviour are investigated. The main findings can be summarised as follows:

- If only unnotched and notched specimens were examined, the material would be classified as fully notch-sensitive, i.e., no support effect. However, the tested local fatigue strength of thin-walled structures is approximately 7% higher than that of the unnotched specimens.
- Both the local assessment concept according to the FKM guideline, based on the material-mechanical support factor, and the point method of the Theory of Critical Distance (TCD), describe this fatigue behaviour of the specimens and the structure well. The FKM approach is conservative, while the TCD overestimates the fatigue strength of the structure by a maximum of 5%.
- The TCD calculations for the 100 μm thin structure are only feasible because the material parameter a_0 is a few micrometres. As this only applies to very high-strength materials, support factor concepts based on the relative stress gradient are more preferable for these kinds of thin-walled structures.
- Regarding the cyclic deformation behaviour, the material shows a very high initial yield strength with subsequent ideal plastic flow during initial loading and distinctly different flow characteristics during reverse loading. A combined hardening approach models this behaviour superbly.
- The numerical simulation of a plastic deformation of the thin structure requires not only the non-linear material behaviour but also the consideration of geometric non-linearity, suitable friction conditions and a realistic mapping of the component dimensions. Geometric influences seem to have a dominant impact and thus obscure the effect of the material model.
- In conclusion, even 100 μm thin structures can be evaluated using conventional specimen fatigue tests and suitable, established fatigue assessment methods. The transferability of the cyclic deformation behaviour appears to be given in principle. This saves future expensive and time-consuming tests of the real structures.

Author Contributions: Conceptualisation, F.H. and G.W.; methodology, F.H. and G.W.; software, F.H.; validation, F.H. and G.W.; formal analysis, F.H.; investigation, F.H.; resources, G.W. and F.G.; data curation, F.H., G.W. and F.G.; writing—original draft preparation, F.H.; writing—review and editing, F.H., G.W., F.G. and C.K.; visualisation, F.H.; supervision, G.W., F.G. and C.K.; project administration, G.W., F.G. and C.K.; funding acquisition, F.G. and C.K. All authors have read and agreed to the published version of the manuscript.

Funding: This research was funded by the Austrian Research Promotion Agency (FFG), grant number 865843.

Institutional Review Board Statement: Not applicable.

Informed Consent Statement: Not applicable.

Data Availability Statement: The data are not publicly available due to a confidentiality agreement.

Acknowledgments: The authors would like to acknowledge the financial support of the “COMET—Competence Centres for Excellent Technologies” Programme of the Austrian Federal Ministry for Climate Action, Environment, Energy, Mobility, Innovation and Technology (BMK) and the Federal Ministry for Digital and Economic Affairs (BMDW) and the Provinces of Styria, Tyrol and Vienna for the COMET Centre (K1) LEC EvoLET. The COMET Programme is managed by the Austrian Research Promotion Agency (FFG).

Conflicts of Interest: The authors declare no conflict of interest.

References

1. Fröschl, J. Fatigue Behaviour of Forged Components: Technological Effects and Multiaxial Fatigue. Ph.D. Thesis, Montanuniversität Leoben, Leoben, Austria, 2006.
2. Gänser, H.P. Strength Assessment of Components Subjected to High-Cycle Fatigue Loading: Linking the Mechanics of Materials and Structures. Habilitation Thesis, Montanuniversität Leoben, Leoben, Austria, 2008.
3. Javidi, A. Influence of Machining on the Surface Integrity and Fatigue Strength of 34CrNiMo6 Steel. Ph.D. Thesis, Montanuniversität Leoben, Leoben, Austria, 2008.
4. Leitner, M. Local Fatigue Assessment of Welded and High Frequency Mechanical Impact Treated Joints. Ph.D. Thesis, Montanuniversität Leoben, Leoben, Austria, 2013.
5. Stoschka, M. Contribution towards Fatigue Strength of Thermo-Mechanically Processed Metallic Components. Habilitation Thesis, Montanuniversität Leoben, Leoben, Austria, 2014.
6. Leitner, M. Technological Aspects in Fatigue Design. Habilitation Thesis, Montanuniversität Leoben, Leoben, Austria, 2019.
7. Rennert, R.; Kullig, E.; Vormwald, M.; Esderts, A.; Siegele, D. *FKM Guideline: Analytical Strength Assessment of Components in Mechanical Engineering Made of Steel, Cast Iron and Aluminium Materials*, 6th ed.; VDMA: Frankfurt, Germany, 2012.
8. Wu, J.H.; Lin, C.K. Tensile and fatigue properties of 17-4 PH stainless steel at high temperatures. *Metall. Mater. Trans. A* **2002**, *33*, 1715–1724. [[CrossRef](#)]
9. Schönbauer, B.M.; Yanase, K.; Endo, M. VHCF properties and fatigue limit prediction of precipitation hardened 17-4PH stainless steel. *Int. J. Fatigue* **2016**, *88*, 205–216. [[CrossRef](#)]
10. Milošević, I.; Renhart, P.; Winter, G.; Grün, F.; Kober, M. Validation of a new high frequency testing technique in the VHCF regime—Fatigue properties of a 42CrMoS4 and X5CrNiCuNb16-4 steel. *Int. J. Fatigue* **2018**, *112*, 198–205. [[CrossRef](#)]
11. Milošević, I.; Garb, C.; Winter, G.; Grün, F.; Kober, M. Effects of Inclusions on the Very High Cycle Fatigue Properties of a High Strength Martensitic Steel within the Transition Area. *Procedia Struct. Integr.* **2017**, *7*, 327–334. [[CrossRef](#)]
12. Nie, D.; Mutoh, Y. Fatigue Limit Prediction of the Matrix of 17-4PH Stainless Steel Based on Small Crack Mechanics. *J. Press. Vessel. Technol.* **2013**, *135*, 397. [[CrossRef](#)]
13. Hsu, K.C.; Lin, C.K. High-temperature fatigue crack growth behavior of 17-4 PH stainless steels. *Metall. Mater. Trans. A* **2004**, *35*, 3018–3024. [[CrossRef](#)]
14. Hsu, K.C.; Lin, C.K. Influence of Frequency on the High-Temperature Fatigue Crack Growth Behavior of 17-4 PH Stainless Steels. *Mater. Trans.* **2007**, *48*, 490–499. [[CrossRef](#)]
15. Schönbauer, B.M.; Yanase, K.; Endo, M. Influence of intrinsic and artificial defects on the VHCF properties of 17-4PH stainless steel. *Procedia Struct. Integr.* **2016**, *2*, 1149–1155. [[CrossRef](#)]
16. Schönbauer, B.M.; Yanase, K.; Endo, M. The influence of various types of small defects on the fatigue limit of precipitation-hardened 17-4PH stainless steel. *Theor. Appl. Fract. Mech.* **2017**, *87*, 35–49. [[CrossRef](#)]
17. Schönbauer, B.M.; Mayer, H. Effect of small defects on the fatigue strength of martensitic stainless steels. *Int. J. Fatigue* **2019**, *127*, 362–375. [[CrossRef](#)]
18. Wu, J.H.; Lin, C.K. Influence of Frequency on High-Temperature Fatigue Behavior of 17-4 PH Stainless Steels. *Mater. Trans.* **2003**, *44*, 713–721. [[CrossRef](#)]
19. Milošević, I.; Winter, G.; Grün, F.; Kober, M. Influence of Size Effect and Stress Gradient on the High-cycle Fatigue Strength of a 1.4542 Steel. *Procedia Eng.* **2016**, *160*, 61–68. [[CrossRef](#)]
20. Himmelbauer, F.; Winter, G.; Grün, F.; Kiesling, C. VHCF properties and assessment of specimens and thin-walled component-like structures made of high-strength steel X5CrNiCuNb16-4. *Int. J. Fatigue* **2022**, *156*, 106645. [[CrossRef](#)]
21. Schönbauer, B.M.; Stanzl-Tschegg, S.E.; Perlega, A.; Salzman, R.N.; Rieger, N.F.; Turnbull, A.; Zhou, S.; Lukaszewicz, M.; Gandy, D. The influence of corrosion pits on the fatigue life of 17-4PH steam turbine blade steel. *Eng. Fract. Mech.* **2015**, *147*, 158–175. [[CrossRef](#)]
22. Carneiro, L.; Jalalahmadi, B.; Ashtekar, A.; Jiang, Y. Cyclic deformation and fatigue behavior of additively manufactured 17-4 PH stainless steel. *Int. J. Fatigue* **2019**, *123*, 22–30. [[CrossRef](#)]
23. Concli, F.; Fraccaroli, L.; Nalli, F.; Cortese, L. High and low-cycle-fatigue properties of 17-4 PH manufactured via selective laser melting in as-built, machined and hipped conditions. *Prog. Addit. Manuf.* **2022**, *7*, 99–109. [[CrossRef](#)]
24. Leitner, M.; Schneller, W.; Springer, S.; Grün, F. Effect of Surface Layer on the Fatigue Strength of Selectively Laser Melted 17-4 PH Steel. *J. Mater. Eng. Perform.* **2021**, *30*, 5383–5391. [[CrossRef](#)]
25. Eichlseder, W. Fatigue analysis by local stress concept based on finite element results. *Comput. Struct.* **2002**, *80*, 2109–2113. [[CrossRef](#)]
26. Taylor, D. Geometrical effects in fatigue: A unifying theoretical model. *Int. J. Fatigue* **1999**, *21*, 413–420. [[CrossRef](#)]
27. Berto, F.; Lazzarin, P. A review of the volume-based strain energy density approach applied to V-notches and welded structures. *Theor. Appl. Fract. Mech.* **2009**, *52*, 183–194. [[CrossRef](#)]
28. Liao, D.; Zhu, S.P. Energy field intensity approach for notch fatigue analysis. *Int. J. Fatigue* **2019**, *127*, 190–202. [[CrossRef](#)]
29. Branco, R.; Costa, J.D.; Borrego, L.P.; Macek, W.; Berto, F. Notch fatigue analysis and life assessment using an energy field intensity approach in 7050-T6 aluminium alloy under bending-torsion loading. *Int. J. Fatigue* **2022**, *162*, 106947. [[CrossRef](#)]
30. Liu, X.; Wang, R.; Hu, D.; Mao, J. A calibrated weakest-link model for probabilistic assessment of LCF life considering notch size effects. *Int. J. Fatigue* **2020**, *137*, 105631. [[CrossRef](#)]

31. He, J.C.; Zhu, S.P.; Tadesse, A.T.; Niu, X. Evaluation of critical distance, highly stressed volume, and weakest-link methods in notch fatigue analysis. *Int. J. Fatigue* **2022**, *162*, 106950. [[CrossRef](#)]
32. Wu, Z.R.; Hu, X.T.; Li, Z.X.; Xin, P.P.; Song, Y.D. Probabilistic fatigue life prediction methodology for notched components based on simple smooth fatigue tests. *J. Mech. Sci. Technol.* **2017**, *31*, 181–188. [[CrossRef](#)]
33. Liao, D.; Zhu, S.P.; Keshtegar, B.; Qian, G.; Wang, Q. Probabilistic framework for fatigue life assessment of notched components under size effects. *Int. J. Mech. Sci.* **2020**, *181*, 105685. [[CrossRef](#)]
34. Spaggiari, A.; Castagnetti, D.; Dragoni, E.; Bulleri, S. Fatigue life prediction of notched components: A comparison between the theory of critical distance and the classical stress-gradient approach. *Procedia Eng.* **2011**, *10*, 2755–2767. [[CrossRef](#)]
35. Mei, J.; Xing, S.; Vasu, A.; Chung, J.; Desai, R.; Dong, P. The fatigue limit prediction of notched components—A critical review and modified stress gradient based approach. *Int. J. Fatigue* **2020**, *135*, 105531. [[CrossRef](#)]
36. Ye, W.L.; Zhu, S.P.; Niu, X.P.; He, J.C.; Wang, Q. Fatigue life prediction of notched components under size effect using stress gradient-based approach. *Int. J. Fract.* **2021**, *126*, 165. [[CrossRef](#)]
37. Leitner, M.; Vormwald, M.; Remes, H. Statistical size effect on multiaxial fatigue strength of notched steel components. *Int. J. Fatigue* **2017**, *104*, 322–333. [[CrossRef](#)]
38. Souto, C.; Gomes, V.; Figueiredo, M.; Correia, J.; Lesiuk, G.; Fernandes, A.A.; de Jesus, A. Fatigue behaviour of thin-walled cold roll-formed steel sections. *Int. J. Fatigue* **2021**, *149*, 106299. [[CrossRef](#)]
39. He, J.C.; Zhu, S.P.; Liao, D.; Niu, X.P. Probabilistic fatigue assessment of notched components under size effect using critical distance theory. *Eng. Fract. Mech.* **2020**, *235*, 107150. [[CrossRef](#)]
40. Luo, P.; Yao, W.; Li, P. A notch critical plane approach of multiaxial fatigue life prediction for metallic notched specimens. *Fatigue Fract. Eng. Mater. Struct.* **2019**, *42*, 854–870. [[CrossRef](#)]
41. Miwa, Y.; Jitsukawa, S.; Hishinuma, A. Development of a miniaturized hour-glass shaped fatigue specimen. *J. Nucl. Mater.* **1998**, *258–263*, 457–461. [[CrossRef](#)]
42. Nozaki, M.; Sakane, M.; Fujiwara, M. Low cycle fatigue testing using miniature specimens. *Int. J. Fatigue* **2020**, *137*, 105636. [[CrossRef](#)]
43. Procházka, R.; Džugan, J. Low cycle fatigue properties assessment for rotor steels with the use of miniaturized specimens. *Int. J. Fatigue* **2022**, *154*, 106555. [[CrossRef](#)]
44. Shin, C.S.; Lin, S.W. Evaluating fatigue crack propagation properties using miniature specimens. *Int. J. Fatigue* **2012**, *43*, 105–110. [[CrossRef](#)]
45. Chandran, K.R.; Cao, F.; Newman, J.C. Fatigue crack growth in miniature specimens: The equivalence of ΔK -correlation and that based on the change in net-section strain energy density. *Scr. Mater.* **2016**, *122*, 18–21. [[CrossRef](#)]
46. Blasón, S.; Werner, T.; Kruse, J.; Madia, M.; Miarka, P.; Seitz, S.; Benedetti, M. Determination of fatigue crack growth in the near-threshold regime using small-scale specimens. *Theor. Appl. Fract. Mech.* **2022**, *118*, 103224. [[CrossRef](#)]
47. Chaboche, J.L. A review of some plasticity and viscoplasticity constitutive theories. *Int. J. Plast.* **2008**, *24*, 1642–1693. [[CrossRef](#)]
48. Chaboche, J.L. Time-independent constitutive theories for cyclic plasticity. *Int. J. Plast.* **1986**, *2*, 149–188. [[CrossRef](#)]
49. ASTM A564; Standard Specification for Hot-Rolled and Cold-Finished Age-Hardening Stainless Steel Bars and Shapes. ASTM International: West Conshohocken, PA, USA, 2013.
50. DIN EN 10088-3; Nichtrostende Stähle—Teil 3: Technische Lieferbedingungen für Halbzeug, Stäbe, Walzdraht, Gezogenen Draht, Profile und Blankstahlerzeugnisse aus korrosionsbeständigen Stählen für allgemeine Verwendung. Beuth Verlag: Berlin, Germany, 2005.
51. Himmelbauer, F.; Tillmanns, M.; Winter, G.; Gruen, F.; Kiesling, C. A novel high-frequency fatigue testing methodology for small thin-walled structures in the HCF/VHCF regime. *Int. J. Fatigue* **2021**, *146*, 106146. [[CrossRef](#)]
52. Milošević, I.; Renhart, P.; Winter, G.; Grün, F.; Kober, M. A new high frequency testing method for steels under tension/compression loading in the VHCF regime. *Int. J. Fatigue* **2017**, *104*, 150–157. [[CrossRef](#)]
53. Dengel, D. Die arc sin \sqrt{P} -Transformation—Ein einfaches Verfahren zur grafischen und rechnerischen Auswertung geplanter Wöhlerversuche [The arc sin \sqrt{P} transformation—A simple method for graphical and computational evaluation of planned Wöhler tests]. *Mater. Und Werkst.* **1975**, *6*, 253–261. [[CrossRef](#)]
54. Dengel, D. Empfehlungen für die statistische Abschätzung des Zeit- und Dauerfestigkeitsverhaltens von Stahl [Recommendations for the statistical estimation of the fatigue strength behavior of steel]. *Mater. Und Werkst.* **1989**, *20*, 73–81. [[CrossRef](#)]
55. Bellett, D.; Taylor, D.; Marco, S.; Mazzeo, E.; Guillois, J.; Pircher, T. The fatigue behaviour of three-dimensional stress concentrations. *Int. J. Fatigue* **2005**, *27*, 207–221. [[CrossRef](#)]
56. El Haddad, M.H.; Topper, T.H.; Smith, K.N. Prediction of non propagating cracks. *Eng. Fract. Mech.* **1979**, *11*, 573–584. [[CrossRef](#)]
57. Halama, R.; Sedlák, J.; Šofer, M. Phenomenological Modelling of Cyclic Plasticity. In *Numerical Modelling*; Miidla, P., Ed.; IntechOpen: London, UK, 2012; pp. 329–354. [[CrossRef](#)]
58. Seisenbacher, B.; Winter, G.; Grün, F. Improved Approach to Determine the Material Parameters for a Combined Hardening Model. *Mater. Sci. Appl.* **2018**, *9*, 357–367. [[CrossRef](#)]
59. Zienkiewicz, O.C.; Taylor, R.L. *The Finite Element Method for Solid and Structural Mechanics*, 6th ed.; Elsevier: Amsterdam, The Netherlands, 2006; Volume 2.
60. Peksen, M. Multiphysics Modelling of Structural Components and Materials. In *Multiphysics Modelling*; Elsevier: Amsterdam, The Netherlands, 2018; pp. 105–138. [[CrossRef](#)]

61. Schönbauer, B.M.; Yanase, K.; Endo, M. Influences of small defects on torsional fatigue limit of 17-4PH stainless steel. *Int. J. Fatigue* **2017**, *100*, 540–548. [[CrossRef](#)]
62. Taylor, D.; Wang, G. The validation of some methods of notch fatigue analysis. *Fatigue Fract. Eng. Mater. Struct.* **2000**, *23*, 387–394. [[CrossRef](#)]
63. Atzori, B.; Meneghetti, G.; Susmel, L. Material fatigue properties for assessing mechanical components weakened by notches and defects. *Fatigue Fract. Eng. Mater. Struct.* **2005**, *28*, 83–97. [[CrossRef](#)]
64. Susmel, L.; Taylor, D. The Theory of Critical Distances as an alternative experimental strategy for the determination of K_{Ic} and ΔK_{th} . *Eng. Fract. Mech.* **2010**, *77*, 1492–1501. [[CrossRef](#)]
65. Askes, H.; Livieri, P.; Susmel, L.; Taylor, D.; Tovo, R. Intrinsic material length, Theory of Critical Distances and Gradient Mechanics: Analogies and differences in processing linear-elastic crack tip stress fields. *Fatigue Fract. Eng. Mater. Struct.* **2013**, *36*, 39–55. [[CrossRef](#)]